

Singularity-Free Inverse Dynamics for Underactuated Systems with a Rotating Mass

Seyed Amir Tafrishi¹, Mikhail Svinin² and Motoji Yamamoto¹

Abstract—Underactuated systems consist of passive bodies/joints that don't have any active torque. To control these systems through inverse dynamics, the inertial coupling creates certain singularities where they are mainly related to constraints that passive bodies impose. In this study, we propose that modeling the trajectory of the rotating mass with multiple phase-shifted sinusoidal curves removes the singularity. At first, we derive the modified non-linear dynamics of a considered rolling system with active torque on the rotating mass by the trajectories of the combined-waves. Also, the inverse dynamics are derived and singularity regions for this underactuated system are demonstrated. Then, we propose a theory that designing the parameters of the combined phase-shifted waves under certain conditions removes the singularity. We obtain this parametric condition from the positive definiteness of the inertia matrix in the inverse dynamics. Finally, the simulation results are confirmed by using a prescribed Beta function on the specified states of the rolling carrier. Because our algebraic method is integrated into the non-linear dynamics, the proposed solution has a great potential to be extended to the Lagrangian mechanics with multiple degrees-of-freedom.

I. INTRODUCTION

Controlling the mechanisms of the machines and robots require an accurate mathematical model of the system. This model should contain all the physical characteristics of the system while it is computationally efficient. However, the control of the underactuated systems with passive bodies have certain challenges that can originate from the derived model [1]. Physically, the underactuated systems [see Fig. 1] consist of two main parts: First, a rotating mass that moves by an actuator. Second, a passive body that displaces depending on the rotational mass.

Early studies for underactuated mechanisms have begun by the introduced Pendubot [2] and Acrobat [3] as the two-link manipulators. The general motion equations of a passive and an active rotating bodies with rotational angles of $\mathbf{q} = [\theta, \gamma]^T$ can be presented as

$$\mathbf{M}(\mathbf{q})\ddot{\mathbf{q}} + \mathbf{h}(\mathbf{q}, \dot{\mathbf{q}}) = \mathbf{u}, \quad (1)$$

where inertial matrix $\mathbf{M}(\mathbf{q})$, velocity dependencies N_i and gravity terms G_i in $\mathbf{h}(\mathbf{q}, \dot{\mathbf{q}})$ and control inputs \mathbf{u} are defined by

$$\mathbf{M}(\mathbf{q}) = \begin{bmatrix} M_{11} & M_{12} \\ M_{21} & M_{22} \end{bmatrix}, \mathbf{h}(\mathbf{q}, \dot{\mathbf{q}}) = \begin{bmatrix} N_1 + G_1 \\ N_2 + G_2 \end{bmatrix}, \mathbf{u} = \begin{bmatrix} 0 \\ \tau_\gamma \end{bmatrix}.$$

The underactuated systems (1) with two degrees of freedom [1] have a great common, similar inertial matrix $\mathbf{M}(\mathbf{q})$, with certain underactuated spherical robots [4]–[7]. This inertial similarity help us to generalize our studying problem. The

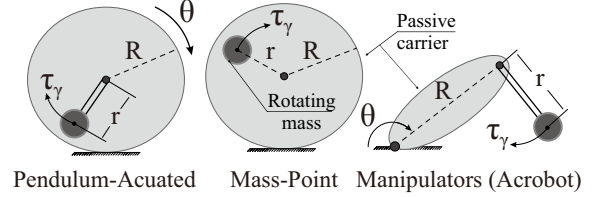


Fig. 1: Different mass-rotating systems with passive body/carrier that their inertial matrices $\mathbf{M}(\mathbf{q})$ are similar.

rolling spherical robots propel their passive carrier with a rotating mass-point [6]–[8] or pendulum [4], [5] as Fig. 1.

From the control point-of-view, Agrawal in 1991 [9] found that when the inertial matrix of the inverse dynamics is singular at certain configurations, the integration of differential equations breaks. Arai and Tachi [10] showed that the inverse dynamics in a two-degree-of-freedom underactuated manipulator hit the singularity when coupled inertia M_{21} term, the first constraint equation imposed from the passive body in (1), becomes zero and this property limits the domain of the control. Spong [11] proposed a Strong Inertial Coupling condition for these underactuated systems under the positive definiteness of the inertia matrix. The condition grants a singular free inverse dynamics under certain geometric properties. In other words, these mathematical singularities that originate from the inversed terms of the inertial matrix $\mathbf{M}(\mathbf{q})$, limit the mechanism to certain geometric parameters and create a challenge in manipulation around these singularity regions. Furthermore, a coupling index was proposed to determine the actuability of underactuated systems with different geometries [12]. Later studies took place by following these coupling conditions [11], [12] for controlling the Pendubot [13] and Acrobat [3], [14]. The same problem was highlighted and control strategies are developed relative to this limitation for spherical robots [5], [7]. Also, because the spherical carrier requires to have consecutive rotations without any angular limitations, the singularities due to inertial coupling become more challenging to deal with.

Our motivation in this letter is to introduce a new theory for modeling the underactuated systems, in which the limitations on the geometric parametrization and configuration singularities due to inertial coupling [11], [12] are avoided. Thus, there wouldn't be any physical design limitations due to mathematical singularities. This modified model is free from any complex algorithm. Additionally, the singularity regions in conventional rolling systems are analyzed for the first time. In this work, we begin by defining the combined phase-shifted curves that construct the circular rotation of mass. Next, the new kinematic model is applied to the Lagrangian equations for finding the rolling spherical carrier's modified dynamics. Then, the inverse dynamics are derived

¹ Seyed Amir Tafrishi and Motoji Yamamoto are with the Department of Mechanical Engineering, Kyushu University, Kyushu, Japan amir@ce.mech.kyushu-u.ac.jp and yama@mech.kyushu-u.ac.jp

² Mikhail Svinin is with the Department of Information Science and Engineering, Ritsumeikan University, Kyoto, Japan svinin@fc.ritsumeikan.ac.jp

and singularity regions are analytically demonstrated for this rolling system. Finally, a theory between combined waves and singularity regions is developed. This condition helps to design our combined waves proportional to the considered physical system. Furthermore, the theoretical findings are verified for a rolling carrier with an actuating mass-point by the simulations. Also, a classic model of the pendulum-actuated system is compared with our modified model to clarify the validity of the theory in simulation space.

For the rest of this paper, we show the kinematics of the combined phase-shifted curves with a rotating mass and also derive the non-linear dynamics in Section II. In Section III, by finding the inverse dynamics, the singularity-free conditions for the obtained model are explained. Finally, Section IV shows example simulations for a mass-point system with obtained singularity-free conditions and compare it with the classical model.

II. MODIFIED DYNAMICAL MODEL

In this section, we introduce sinusoidal trajectories that are combined around a circle. Next, the developed kinematics for a rotating mass is substituted into the Lagrangian function of a rolling system. Finally, the Lagrangian method is utilized to find the nonlinear dynamics of this underactuated model. The constructed trajectory with combined waves decomposes the terms of the non-linear model to sub-terms for each wave. Using this property, we will propose a theory that the singularities due to inertial coupling are removed through designing these combined waves.

A. Trajectory with Combined Sinusoidal Waves

Let us assume that the rotating mass has an orientation angle of γ with respect to the center of the spherical carrier with a radius of R [see Fig. 2]. Also, the carrier is rolling with an angle of θ . Then, the following position vector is defined by a sinusoidal curve on the circle with a radius of r as

$$\mathbf{D}_w = -[(r + a \sin n(\gamma + \theta)) \cos(\gamma + \theta)] \mathbf{k} - [(r + a \sin n(\gamma + \theta)) \sin(\gamma + \theta)] \mathbf{j}, \quad (2)$$

where a and n are the amplitude of sinusoidal wave and the frequency of created periodic wave on the circle of radius r , respectively. In the classic mass-rotating models, this trajectory becomes

$$\mathbf{D}_w = -r(\cos(\gamma + \theta) \mathbf{k} + \sin(\gamma + \theta) \mathbf{j}) \quad (3)$$

where a and n are zero in (2) that gives a circular rotation with radius r [6], [15]. In our modified model, Eq. (2) is extended to l sinusoidal waves where the mean creates the trajectory \mathbf{D}_c on circular reference path r as

$$\mathbf{D}_c = \frac{1}{l} \sum_{i=1}^l [-((r + a_i \sin(n_i(\gamma + \theta) + \varepsilon_i)) \cos(\gamma + \theta)) \mathbf{k} - ((r + a_i \sin(n_i(\gamma + \theta) + \varepsilon_i)) \sin(\gamma + \theta)) \mathbf{j}], \quad (4)$$

where $n_i = l n'_i$ and $\varepsilon_i = [(2\pi i)/l]$ are the frequency and phase shift of the i th wave. Note that n'_i is a constant multiplier of wave's frequency. Here, i th circular wave has the phase shift ε_i where it is expected to combine l number of these circular waves for having a constant circle with radius r . We aim to design n_i , a_i and l depending on the obtained relations from the inertial matrix to removes the

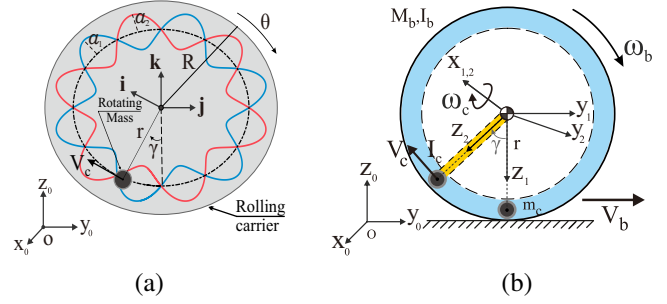


Fig. 2: a) A rotating mass with the trajectory of combined phase-shifted waves on a circle with radius r . Note that the dashed-black line shows the resultant constant radius r from a combination of the two waves with a π phase difference. b) Rolling carrier motion along y axis and frame transformations.

coupling singularity¹ while rotating mass follows r radius circle. Also, the deviation of trajectory \mathbf{D}_c with respect to circular radius r can be found as

$$\Delta D_c = r - \|\mathbf{D}_c\| = \frac{1}{l} \sum_{i=1}^l a_i \sin(n_i(\gamma + \theta) + \varepsilon_i), \quad (5)$$

where $\|\cdot\|$ stands for the module of the complex variable. To have a circular rotation, we can easily prove from (5) that deviation always is $\Delta D_c = 0$ assuming $a_i = a$ and $n_i = n$ are constant values for l waves [see example for $l = 2$ phase case with $a = a_1 = a_2$ and $n = n_1 = n_2$ in Fig. 2-a], so

$$\Delta D_c = a \left[\sin \left(n(\gamma + \theta) + \frac{2\pi(1)}{l} \right) + \sin \left(n(\gamma + \theta) + \frac{2\pi(2)}{l} \right) + \dots + \sin \left(n(\gamma + \theta) + \frac{2\pi(l)}{l} \right) \right] = 0. \quad (6)$$

From the sine summations in (6), any l number of the waves will always equal to zero. Thus, with considered assumption ($a_i = a$ and $n_i = n$) for designing the waves, Eq. (4) becomes

$$\begin{aligned} \mathbf{D}_c &= -\frac{\cos(\gamma + \theta) \mathbf{k} + \sin(\gamma + \theta) \mathbf{j}}{l} \sum_{i=1}^l r + a_i \sin(n_i(\gamma + \theta) + \varepsilon_i) \\ &= -\frac{\cos(\gamma + \theta) \mathbf{k} + \sin(\gamma + \theta) \mathbf{j}}{l} (lr + \Delta D_c) = \mathbf{D}_w|_{a=n=l=0} \end{aligned} \quad (7)$$

Note that $\Delta D_c = 0$ as (6), hence, we will always have the circular trajectory with fixed radius r (3) similar to the classic rotating mass systems. This proves that after deriving our general model by Eq. (4) and determining the required values for wave variables, combining these artificial waves will result a constant circular rotation with radius r .

To find the rolling kinematics, the coordinate frames are sketched as Fig. 2-b. Here, $x_0 y_0 z_0$ represents the reference frame. The moving frame connected to the center of the spherical carrier is $x_1 y_1 z_1$, which translates with respect to reference frame $x_0 y_0 z_0$. Finally, $x_2 y_2 z_2$ is a rotating frame for the rotating mass-point attached to the center of spherical carrier and it is rotating with respect to $x_1 y_1 z_1$. The corresponding kinematics for a rolling carrier with rotational

¹Please check Theorem 1 for details.

mass is

$$\boldsymbol{\omega}_b = \dot{\theta} \mathbf{i}, \mathbf{V}_b = R\dot{\theta} \mathbf{j}, \boldsymbol{\omega}_c = (\dot{\gamma} + \dot{\theta}) \mathbf{i}, \mathbf{V}_c = \mathbf{V}_b + \dot{\mathbf{D}}_c \quad (8)$$

where $\boldsymbol{\omega}_b$, \mathbf{V}_b , $\boldsymbol{\omega}_c$ and \mathbf{V}_c are the angular and linear velocities of the carrier and the angular and linear velocities of the rotating mass. Also, the linear velocity of the rotating mass \mathbf{V}_c is obtained by differentiating the Eq. (4) as

$$\begin{aligned} \mathbf{V}_c = & [R\dot{\theta} - \frac{\dot{\gamma} + \dot{\theta}}{l} \sum_{i=1}^l [(a_i n_i \cos(n_i(\gamma + \theta) + \varepsilon_i)) \sin(\gamma + \theta) \\ & + (r + a_i \sin(n_i(\gamma + \theta) + \varepsilon_i)) \cos(\gamma + \theta)] \mathbf{j} \\ & - \frac{\dot{\gamma} + \dot{\theta}}{l} \sum_{i=1}^l [a_i n_i \cos(n_i(\gamma + \theta) + \varepsilon_i) \cos(\gamma + \theta) \\ & - (r + a_i \sin(n_i(\gamma + \theta) + \varepsilon_i)) \sin(\gamma + \theta)] \mathbf{k}. \end{aligned} \quad (9)$$

B. Nonlinear Dynamics

The non-linear dynamics of the rolling spherical carrier with a planar motion is derived from the proposed trajectory equation. To find the corresponding motion equations, the Lagrangian equations are utilized.

We consider a sphere as a passive carrier (passive joint) where it is actuated with the rotation of a spherical mass as Fig. 2. The carrier has a mass of M_b excluding the rotating mass. Also, the rotating mass with the mass m_c is assumed as a mass-point. The Lagrangian function of the rolling carrier with the rotating mass, including kinetic and potential energies, along y axis is described [15] as follows

$$\begin{aligned} E_L = & \frac{1}{2} M_b \|\mathbf{V}_b\|^2 + \frac{1}{2} I_b \|\boldsymbol{\omega}_b\|^2 + \frac{1}{2} m_c \|\mathbf{V}_c\|^2 \\ & + \frac{1}{2} I_c \|\boldsymbol{\omega}_c\|^2 - m_c g d_c, \end{aligned} \quad (10)$$

where $I_b = 2M_b R^2/3$, I_c , g and d_c are the inertia tensor of rolling passive carrier, an arbitrary inertia tensor I_c connected to the mass-point, the acceleration of gravity and the distance of the mass-point respect to the ground, respectively. We include the inertia tensor I_c for the sake of generality that its rotation is with the respect to carrier central frame $x_1 y_1 z_1$. This arbitrary inertia tensor I_c can be considered as either the lead of rotating pendulum [4], [5] (yellow pendulum in Fig. 2) or interacting fluid/gas inside pipes for the rotating spherical mass [7] (blue fluid/gas in Fig. 2). After the substitution of Eqs. (8)-(9) into (10), one obtains

$$\begin{aligned} E_L = & \frac{1}{2} R^2 \dot{\theta}^2 M_b + \frac{1}{2} I_b \dot{\theta}^2 + \frac{1}{2} I_c (\dot{\gamma}^2 + \dot{\theta}^2) + \frac{1}{2} m_c \left[[R\dot{\theta} \right. \\ & - \frac{\dot{\gamma} + \dot{\theta}}{l} \sum_{i=1}^l (a_i n_i \cos(n_i(\gamma + \theta) + \varepsilon_i)) \sin(\gamma + \theta) \\ & + (r + a_i \sin(n_i(\gamma + \theta) + \varepsilon_i)) \cos(\gamma + \theta)]^2 \\ & + [a_i n_i \cos(n_i(\gamma + \theta) + \varepsilon_i) \cos(\gamma + \theta) \\ & - (r + a_i \sin(n_i(\gamma + \theta) + \varepsilon_i)) \sin(\gamma + \theta)]^2 \Big] \\ & - \frac{m_c}{l} \sum_{i=1}^l g [r + a_i \sin(n_i(\gamma + \theta) + \varepsilon_i)] (1 - \cos(\gamma + \theta)) \end{aligned} \quad (11)$$

Finally, we apply the Lagrangian equations for planar translation along y axis as following

$$\frac{d}{dt} \left(\frac{\partial E_L}{\partial \dot{\gamma}} \right) - \frac{\partial E_L}{\partial \gamma} = \tau_\gamma, \quad \frac{d}{dt} \left(\frac{\partial E_L}{\partial \dot{\theta}} \right) - \frac{\partial E_L}{\partial \theta} = \tau_\theta, \quad (12)$$

where τ_γ and τ_θ are the external torques for the rotating mass and the sphere. Acting external torque between the surfaces of the spherical mass and carrier body is assumed zero, $\tau_\theta = 0$, since mass-point doesn't contain any spinning around itself and it only rotates with the respect to the carrier center $x_1 y_1 z_1$. After doing the necessary operations by Eqs. (11)-(12), the terms of the equations of the motion (1) for this underactuated system becomes

$$\begin{aligned} M_{11} = & I_c + M_b R^2 + I_b + m_c R^2 - 2m_c R \mu_1 + m_c \mu_2, \\ M_{12} = & M_{21} = I_c - m_c R \mu_1 + m_c \mu_2, \\ M_{22} = & I_c + m_c \mu_2, \\ N_1 = & -m_c R (\dot{\gamma} + \dot{\theta})^2 \mu_3 + m_c (\dot{\gamma} + \dot{\theta})^2 \mu_4, \\ N_2 = & m_c (\dot{\gamma} + \dot{\theta})^2 \mu_4, \\ G_1 = & G_2 = m_c g \mu_5. \end{aligned} \quad (13)$$

while,

$$\begin{aligned} \mu_1 = & \frac{1}{l} \sum_{i=1}^l (a_i n_i \cos(n_i(\gamma + \theta) + \varepsilon_i)) \sin(\gamma + \theta) \\ & + (r + a_i \sin(n_i(\gamma + \theta) + \varepsilon_i)) \cos(\gamma + \theta), \\ \mu_2 = & \frac{1}{l} \sum_{i=1}^l a_i^2 n_i^2 \cos^2(n_i(\gamma + \theta) + \varepsilon_i) \\ & + (r + a_i \sin(n_i(\gamma + \theta) + \varepsilon_i))^2, \\ \mu_3 = & \frac{1}{l} \sum_{i=1}^l -a_i n_i^2 \sin(n_i(\gamma + \theta) + \varepsilon_i) \sin(\gamma + \theta) \\ & + 2a_i n_i \cos(n_i(\gamma + \theta) + \varepsilon_i) \cos(\gamma + \theta) \\ & - (r + a_i \sin(n_i(\gamma + \theta) + \varepsilon_i)) \sin(\gamma + \theta), \\ \mu_4 = & \frac{1}{l} \sum_{i=1}^l -a_i^2 n_i^3 \sin(n_i(\gamma + \theta) + \varepsilon_i) \cos(n_i(\gamma + \theta) + \varepsilon_i) \\ & + a_i n_i \cos(n_i(\gamma + \theta) + \varepsilon_i) (r + a_i \sin(n_i(\gamma + \theta) + \varepsilon_i)) \\ \mu_5 = & \frac{1}{l} \sum_{i=1}^l a_i n_i \cos(n_i(\gamma + \theta) + \varepsilon_i) (1 - \cos(\gamma + \theta)) \\ & + (r + a_i \sin(n_i(\gamma + \theta) + \varepsilon_i)) \sin(\gamma + \theta). \end{aligned} \quad (14)$$

Note that due to the linearity property of the summations, we can now interpret each wave $(a_i, n_i, \varepsilon_i)$ in Eq. (13) as a separate particle model in terms that the total average of these particles creates the dynamics of the rotating mass in a relation to the rolling carrier.

III. INVERSE DYNAMICS AND SINGULARITY

In this section, the non-linear dynamics are presented in inverse form. A general condition for removing the singularity is derived and the singularity regions are analyzed for example systems. Next, we propose our theory for determining the parameters of the combined waves to avoid the singularity regions that originate from the coupled inertia

matrix. Finally, a Beta function as feed-forward control for specifying the spherical carrier rotation is given.

The non-linear dynamics (1) with Eq. (13) are re-ordered with the goal to find the input torque τ_γ from the specified rolling carrier states $(\theta, \dot{\theta}, \ddot{\theta})$. Hence, the rolling constraint of the carrier and the rotating mass differential equations in Eq. (1) becomes

$$\begin{aligned}\ddot{\gamma} &= -\frac{1}{M_{12}} (M_{11}\ddot{\theta} + N_1 + G_1), \\ \tau_\gamma &= M_{21}\ddot{\theta} + M_{22}\ddot{\gamma} + N_2 + G_2.\end{aligned}\quad (15)$$

Now, we knew from (1) that inertial matrix $\mathbf{M}(q)$ is always a positive definite and symmetric matrix [9] where upper-left determinants grant this condition by $M_{11} > 0$ and $M_{11}M_{22} - M_{12}M_{21} > 0$. To extend these conditions to the derived inverse dynamics, the rolling constraint (first differential equation) in Eq. (15) is substituted into the second differential equation as follows

$$\bar{\tau}_\gamma = \bar{M}\ddot{\theta} + \bar{N} + \bar{G}, \quad (16)$$

where

$$\begin{aligned}\bar{\tau}_\gamma &= -\tau_\gamma, \quad \bar{M} = M_{12}^{-1} \cdot (M_{11}M_{22} - M_{12}M_{21}), \\ \bar{N} &= M_{22}M_{12}^{-1}N_1 - N_2, \quad \bar{G} = M_{22}M_{12}^{-1}G_1 - G_2.\end{aligned}\quad (17)$$

Because the mass-point and the carrier rotation are opposite of each other in our motion and for the sake of the simplicity, we assume $\bar{\tau}_\gamma = -\tau_\gamma$. By relying on the Ref. [11], the coupled inertia matrix $\bar{M} > 0$ should be positive definite as well. However, denominator in $\bar{M} > 0$ requires another extra condition that $M_{12}^{-1} > 0$. Thus, under the condition of $M_{11}M_{22} - M_{12}M_{21} > 0$, there exist singularities in the solution of Eq. (16) for the cases when $M_{12} \leq 0$ ($\tau_\gamma \rightarrow \infty$) [9]. Thus, following proposition as the condition of the singularity is expressed.

Proposition 1 *Let the inverse non-linear dynamics (16)-(17) are the rolling system with the trajectory of \mathbf{D}_c in (4). Given $M_{12} > 0$, the underactuated system does not hit any singularity, if following condition is satisfied*

$$\mu_{1a}^2 + \mu_{1b}^2 + \frac{I_c}{m_c} > R[\mu_{1a} \sin(\gamma + \theta) + \mu_{1b} \cos(\gamma + \theta)], \quad (18)$$

where μ_{1a} and μ_{1b} are the first and second terms of μ_1 .

Proof: Consider the inertia term M_{12} in (17) always positive to the avoid singularity

$$M_{12} = I_c - m_c R \mu_1 + m_c \mu_2 > 0. \quad (19)$$

Then, μ_{1a} and μ_{1b} terms are defined from μ_1 in (14) as

$$\begin{aligned}\mu_{1a} &= \frac{1}{l} \sum_{i=1}^l a_i n_i \cos(n_i(\gamma + \theta) + \varepsilon_i) \\ \mu_{1b} &= \frac{1}{l} \sum_{i=1}^l r + a_i \sin(n_i(\gamma + \theta) + \varepsilon_i).\end{aligned}$$

where there are $\mu_2 = \mu_{1a}^2 + \mu_{1b}^2$ and $\mu_1 = \mu_{1a} \sin(\gamma + \theta) + \mu_{1b} \cos(\gamma + \theta)$. Then, μ_{1a} and μ_{1b} are substituted to inequality (19) as follows

$$\begin{aligned}m_c(\mu_{1a}^2 + \mu_{1b}^2) - m_c R(\mu_{1a} \sin(\gamma + \theta) \\ + \mu_{1b} \cos(\gamma + \theta)) + I_c > 0\end{aligned}\quad (20)$$

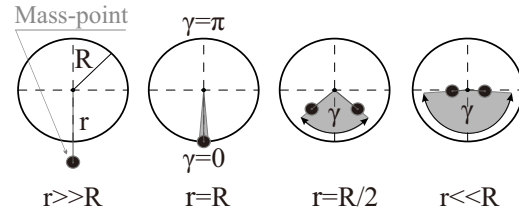


Fig. 3: Singularity regions in gray color increases as mass-point distance r decreases while the carrier is steady ($\theta = 0$).

Finally, the condition (18) is found by reordering inequality (20). ■

Before designing our combined-waves model under the Proposition 1, we check the singularity regions for the different classical underactuated rolling systems. Note that in these cases the trajectory is considered as an ideal circle (3) without any consideration of our combined sinusoidal curves.

Example 1 *Singularity region of a classical rotating mass-point system [6], [15], where $I_c = 0$, are analyzed using condition (18) in Proposition 1. Let the trajectory \mathbf{D}_c be a perfect circle with radius r , which makes $\mu_{1a} = 0$ and $\mu_{1b} = r$ as (3) when $a_i = n_i = \varepsilon_i = 0$. From the given (18) condition, the inequality is transformed to*

$$r^2 > Rr \cos(\gamma + \theta) \quad (21)$$

Now, by considering the maximum possible value for $\cos(\gamma + \theta) \approx 1$, one obtains a limitation on the geometric parametrization as

$$\frac{r}{R} > 1. \quad (22)$$

This means in designing this mass-point system, the inverse dynamics model (15) will hit singularity if the radius of rotating mass be less than rolling carrier as condition (22) and singularity disobeys the physical mechanics completely. Fig. 3 shows how changes in the geometric parameters (r, R) in (21) affect singular configurations of the mass-point (3) on the steady spherical carrier ($\theta = 0$). This graphic clarifies that rolling systems without any angular constraint on γ and θ will hit the singularity. Otherwise, the solution of (15) will break many times while this singular region changes by spherical carrier rotation, $\gamma + \theta$.

Example 2 *A rotating mass system with arbitrary inertial tensor is chosen in this example. This inertia tensor I_c can be related to a rod that connects the mass to the center of the rolling body [4], [5] or an interacted water with the rotating mass in pipes [6], [7]. Thus, with a circular trajectory as the previous example, condition (22) is transformed to*

$$m_c r^2 + I_c > m_c R r \cos(\gamma + \theta), \quad (23)$$

By sorting this condition based on the I_c with considering $\cos(\gamma + \theta) \approx 1$, we see that singularity can be avoided only when

$$I_c > m_c r(R - r). \quad (24)$$

Similar to the previous example, singularity limits the inverse dynamics for only certain mechanisms that can satisfy the following geometric condition.

To show that our proposed approach removes the demonstrated singularity regions in Eq. (21) and Eq. (23), and how parameters of the combined waves should be designed analytically a theory is developed.

Theorem 1 *The trajectory with multiple combined sinusoidal waves never hit singularity and positive definiteness of $\bar{M} > 0$ is granted when variables a_i and n_i of the combined waves in this model are designed for $l > 2$ with satisfying following inequalities*

$$\begin{aligned} \frac{1}{l} \sum_{i=1}^l r^2 + \frac{a_i^2}{2} [n_i^2 + (n_i^2 - 1) \cos 2\varepsilon_i + 1] + \frac{I_c}{m_c} &> \Delta\mu_1 \\ \frac{1}{l} \sum_{i=1}^l r^2 + \frac{a_i^2}{2} [n_i^2 + (n_i^2 - 1) \cos 2\varepsilon_i + 1] + \frac{I_c}{m_c} &> \frac{\sqrt{2}}{2} Rr + \Delta\mu_2 \\ \frac{1}{l} \sum_{i=1}^l r^2 + \frac{a_i^2}{2} [n_i^2 + (n_i^2 - 1) \cos 2\varepsilon_i + 1] + \frac{I_c}{m_c} &> Rr + \Delta\mu_3 \end{aligned} \quad (25)$$

where

$$\begin{aligned} \Delta\mu_1 &= a_i \cdot \left| 2r \sin \left(\tan^{-1} \left(\frac{-2r}{Rn_i} \right) \right) - Rn_i \cos \left(\tan^{-1} \left(\frac{-2r}{Rn_i} \right) \right) \right|, \\ \Delta\mu_2 &= \frac{\sqrt{2}a_i}{2} \left| (2\sqrt{2}r - R) \sin \left(\tan^{-1} \left((R - 2\sqrt{2}r) / Rn_i \right) \right) \right. \\ &\quad \left. - Rn_i \cos \left(\tan^{-1} \left((R - 2\sqrt{2}r) / Rn_i \right) \right) \right|, \\ \Delta\mu_3 &= a_i \cdot |2r - R|. \end{aligned}$$

Proof: Let the singularity condition (18) from Proposition 1 be

$$\mu_{1a}^2 + \mu_{1b}^2 + \frac{I_c}{m_c} > R(\mu_{1a} \sin(\gamma + \theta) + \mu_{1b} \cos(\gamma + \theta)).$$

To have the right-hand side of the inequality always larger than the left-side, we find the absolute value of left-side in the three cases as

$$\begin{aligned} 1) \mu_{1a}^2 + \mu_{1b}^2 + \frac{I_c}{m_c} &> R \cdot |\mu_{1a}|, & \text{for } \zeta_1 = \frac{(k+1)\pi}{2} \\ 2) \mu_{1a}^2 + \mu_{1b}^2 + \frac{I_c}{m_c} &> \frac{\sqrt{2}R}{2} \cdot (|\mu_{1a}| + |\mu_{1b}|), & \text{for } \zeta_2 = \frac{(k+1)\pi}{4} \\ 3) \mu_{1a}^2 + \mu_{1b}^2 + \frac{I_c}{m_c} &> R \cdot |\mu_{1b}|, & \text{for } \zeta_3 = (k+1)\pi \end{aligned} \quad (26)$$

where $\zeta_i = \gamma + \theta$. Next, we utilize the Fourier Transform equations [16] as follows

$$\begin{aligned} H(w) &= \frac{1}{\sqrt{2\pi}} \int_{-\infty}^{\infty} \mu(\zeta_i) e^{-jw\zeta_i} d\zeta_i, \\ \mu(\zeta_i) &= \frac{1}{\sqrt{2\pi}} \int_{-\infty}^{\infty} H(w) e^{jw\zeta_i} dw, \end{aligned} \quad (27)$$

where $H(w)$ and w are the transformed term of μ and the frequency of corresponding μ . With applying Fourier Transform (27) to each side of inequalities in (26) under linearity property [16], one obtains

$$\begin{aligned} 1) H_{1a}^2 + H_{1b}^2 + \frac{I_c'(w)}{m_c} &> R \cdot |H_{1a}|, \\ 2) H_{1a}^2 + H_{1b}^2 + \frac{I_c'(w)}{m_c} &> \frac{\sqrt{2}R}{2} \cdot (|H_{1a}| + |H_{1b}|), \\ 3) H_{1a}^2 + H_{1b}^2 + \frac{I_c'(w)}{m_c} &> R \cdot |H_{1b}|, \end{aligned} \quad (28)$$

where $I_c'(w)$ is the Fourier Transform of the inertia tensor of I_c , while the relevant terms are

$$\begin{aligned} H_{1a}^2 + H_{1b}^2 &= \frac{1}{l} \sum_{i=1}^l \pi(a_i^2 n_i^2 + a_i^2 + 2r^2) \delta(w) \\ &\quad + \frac{\pi a_i^2 (n_i^2 - 1)}{2} [e^{-2j\varepsilon_i} \delta(2n_i + w) + e^{2j\varepsilon_i} \delta(2n_i - w)] \\ &\quad + 2\pi a_i r [e^{-j\varepsilon_i} \delta(n_i + w) - e^{j\varepsilon_i} \delta(n_i - w)] j, \\ |H_{1a}| &= \frac{1}{l} \sum_{i=1}^l \pi a_i n_i [e^{-j\varepsilon_i} \delta(n_i + w) + e^{j\varepsilon_i} \delta(n_i - w)], \\ |H_{1b}| &= 2\pi r \delta(w) + \frac{1}{l} \sum_{i=1}^l \pi a_i [e^{-j\varepsilon_i} \delta(n_i + w) \\ &\quad - e^{j\varepsilon_i} \delta(n_i - w)] j, \end{aligned} \quad (29)$$

By using transformed equation (29), the combined waves are simplified to two base waves for comparison: the first term is the constant shift by $\delta(w)$ and the second is the sinusoidal waves, $\delta(n_i + w) + \delta(n_i - w)$. Because the angular rotation $\zeta(\gamma, \theta)$ of the waves in both sides of inequality is always same, each side of (28) can be compared relative to its multiplier δ with the same frequency w . As an interesting point, despite the usage of waves in different phases ε_i , they are simply canceled out from both sides of inequality (28) with the help of Fourier Transformation [16]. By the known insight in the expressed properties, all three conditions in (28) are collected for each specific impulse δ in the given frequency w in i th wave in the following form

$$\begin{aligned} 1) \left\{ \begin{array}{l} \delta(w) : \pi(a_i^2 n_i^2 + a_i^2 + 2r^2) > 0, \\ e^{-j\varepsilon_i} \delta(n_i + w) : 2rj > Rn_i, \\ -e^{j\varepsilon_i} \delta(n_i - w) : 2rj > -Rn_i, \end{array} \right. \\ 2) \left\{ \begin{array}{l} \delta(w) : \pi(a_i^2 n_i^2 + a_i^2 + 2r^2) > \sqrt{2}\pi Rr, \\ e^{-j\varepsilon_i} \delta(n_i + w) : 4rj > \sqrt{2}R(n_i + j), \\ -e^{j\varepsilon_i} \delta(n_i - w) : 4rj > -\sqrt{2}R(n_i - j), \end{array} \right. \\ 3) \left\{ \begin{array}{l} \delta(w) : \pi(a_i^2 n_i^2 + a_i^2 + 2r^2) > 2\pi Rr, \\ e^{-j\varepsilon_i} \delta(n_i + w) : 2r > R, \\ -e^{j\varepsilon_i} \delta(n_i - w) : 2r > R, \end{array} \right. \end{aligned} \quad (30)$$

To keep the left-hand side always be larger than the right-hand side of inequalities, the moduli (presented like $\|x + jy\| = \sqrt{x^2 + y^2}$) of these complex transforms (30) are calculated

$$\begin{aligned} 1) \left\{ \begin{array}{l} \|\delta(w)\| : \pi(a_i^2 n_i^2 + a_i^2 + 2r^2) > 0, \\ \|e^{-j\varepsilon_i} \delta(n_i + w) + e^{j\varepsilon_i} \delta(n_i - w)\| : 2r > Rn_i \end{array} \right. \\ 2) \left\{ \begin{array}{l} \|\delta(w)\| : \pi(a_i^2 n_i^2 + a_i^2 + 2r^2) > 2\sqrt{2}\pi Rr, \\ \|e^{-j\varepsilon_i} \delta(n_i + w) + e^{j\varepsilon_i} \delta(n_i - w)\| : 4r > \sqrt{2}R(n_i^2 + 1)^{\frac{1}{2}} \end{array} \right. \\ 3) \left\{ \begin{array}{l} \|\delta(w)\| : \pi(a_i^2 n_i^2 + a_i^2 + 2r^2) > 2\pi Rr, \\ \|e^{-j\varepsilon_i} \delta(n_i + w) + e^{j\varepsilon_i} \delta(n_i - w)\| : 2r > R. \end{array} \right. \end{aligned} \quad (31)$$

Because, the amplitudes of the combined waves doesn't give clear comparison, the conditions are extended by the phase difference between each of the sides. Thus, by checking (30), we see that there are $\pi/2$ and $\pi/4$ phase differences between each side of sinusoidal curves in conditions 1 and 2, respectively. Then, the sinusoidal parts of the waves are

represented from (30)-(31)

$$\begin{aligned} 1) & \left\{ \begin{aligned} 2rj(e^{-j\varepsilon_i}\delta(n_i+w) - e^{j\varepsilon_i}\delta(n_i-w)) &> Rn_i[e^{-j\varepsilon_i} \\ &\delta(n_i+w) + e^{j\varepsilon_i}\delta(n_i-w)] \end{aligned} \right. \\ 2) & \left\{ \begin{aligned} 4rj(e^{-j\varepsilon_i}\delta(n_i+w) - e^{j\varepsilon_i}\delta(n_i-w)) &> \sqrt{2}R[e^{-j\varepsilon_i} \\ &\delta(n_i+w)(n_i+j) + e^{j\varepsilon_i}\delta(n_i-w)(n_i-j)] \end{aligned} \right. \\ 3) & \left\{ \begin{aligned} 2rj(e^{-j\varepsilon_i}\delta(n_i+w) - e^{j\varepsilon_i}\delta(n_i-w)) &> Rj[e^{-j\varepsilon_i}\delta(n_i \\ &+w) - e^{j\varepsilon_i}\delta(n_i-w)] \end{aligned} \right. \end{aligned} \quad (32)$$

By taking the Inverse Fourier Transform from (32) and calculating the required shifts of each comparison, the minimum shift requirements $\Delta\mu$ [see the Appendix for derivations], for a right-hand side larger than the left-hand, are calculated

$$\begin{aligned} 1) \Delta\mu_1 &= a_i \cdot \left| 2r \sin \left(\tan^{-1} \left(\frac{-2r}{Rn_i} \right) \right) - Rn_i \cos \left(\tan^{-1} \left(\frac{-2r}{Rn_i} \right) \right) \right| \\ 2) \Delta\mu_2 &= \frac{\sqrt{2}a_i}{2} \left| (2\sqrt{2}r - R) \sin \left(\tan^{-1} \left(\frac{(R - 2\sqrt{2}r)}{Rn_i} \right) \right) \right. \\ &\quad \left. - Rn_i \cos \left(\tan^{-1} \left(\frac{(R - 2\sqrt{2}r)}{Rn_i} \right) \right) \right| \\ 3) \Delta\mu_3 &= a_i \cdot |2r - R| \end{aligned} \quad (33)$$

By substituting Eq. (31) and Eq. (33) back to inequality (28) and taking the Inverse Fourier for single wave i , one obtains

$$\begin{aligned} 1) & \frac{a_i^2(n_i^2+1)}{2} + \frac{a_i^2(n_i^2-1)}{2} \cos(2(n_i\zeta_1 + \varepsilon_i)) + r^2 \\ & + \frac{I_c}{m_c} > \Delta\mu_1(a_i, n_i), \\ 2) & \frac{a_i^2(n_i^2+1)}{2} + \frac{a_i^2(n_i^2-1)}{2} \cos(2(n_i\zeta_2 + \varepsilon_i)) + r^2 \\ & + \frac{I_c}{m_c} > \frac{\sqrt{2}}{2}Rr + \Delta\mu_2(a_i, n_i), \\ 3) & \frac{a_i^2(n_i^2+1)}{2} + \frac{a_i^2(n_i^2-1)}{2} \cos(2(n_i\zeta_3 + \varepsilon_i)) + r^2 \\ & + \frac{I_c}{m_c} > Rr + \Delta\mu_3(a_i, n_i), \end{aligned} \quad (34)$$

To simplify the second term at right-hand side of inequalities (34), we assume that always $l > 2$ which results to transfer $\cos(2(n_i\zeta + \varepsilon_i))$ to $\cos 2\varepsilon_i$ in all conditions $\{\zeta_1, \zeta_2, \zeta_3\}$. Under the given assumption ($l > 2$), the Eq. (25) can be derived from (34) with including l combined waves summation. ■

Remark 1 Because inertia tensor I_c of the rotating mass is normally related to geometric objects (connecting cylindrical bar of pendulum) with a constant radius, it has been included as the constant value to the inequality.

Remark 2 This Theory 1 can easily be extended for any underactuated system with two-link manipulators (for example the Acrobat) since M_{12} term is in common in all models and does not have the inertia tensor of carrier I_b .

In this study, we choose a 4th order Beta function [5], [7] to arrive the carrier $\theta(t)$ toward its desired final configurations θ_{des} by

$$\theta(t) = k \left(-\frac{20}{T^7}t^7 + \frac{70}{T^6}t^6 - \frac{84}{T^5}t^5 + \frac{35}{T^4}t^4 \right), \quad (35)$$

where T and k are the time constant of designed motion and the value for the final arrived distance $\theta(T) = k = \theta_{des}$. We

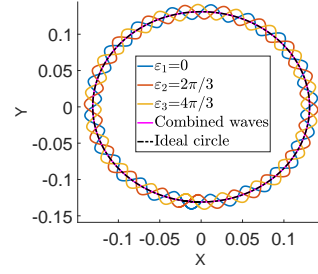


Fig. 4: Geometric shape of combined waves on the trajectory for the rotating mass. Note that the combined waves resultant trajectory always align with ideal rotating mass circle r .

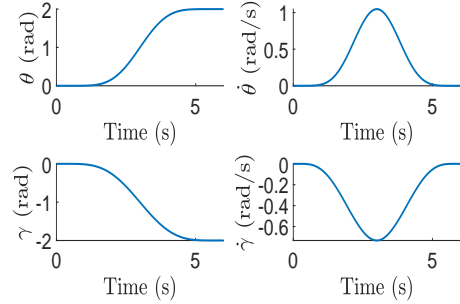


Fig. 5: Example simulation for passive carrier $\{\theta, \dot{\theta}\}$ and rotating mass-point $\{\gamma, \dot{\gamma}\}$ states by the modified model.

expect from this feed-forward control to actuate the rotating mass like $\gamma(t) = d^2\theta(t)/dt^2$ from (35) as a two-step motion. This two-step motion of rotating mass [see $\gamma + \theta$ at Fig. 6-b as an example of this motion pattern] is followed by a counterclockwise rotation till certain angle γ_{max} and a similar clockwise rotation for returning to the rest position. Note that similar to what has been developed in [5], [7], one can show that with the selection of this motion scenario the condition $\dot{\theta}(T) = 0$ is always satisfied.

IV. SIMULATION ANALYSIS

In this section, the proposed theory is analyzed in the simulation space. At first, to evaluate the condition in the worst-case scenario, a mass-point system with $I_c = 0$ is chosen. We find the singular-free model with satisfying the proposed Theorem that uses the combined phase-shifted waves. Next, to show that the modified model is similar to the classic model, we compare both cases when there is an inertia tensor I_c as a pendulum system.

Matlab ODE45 is used during the simulation studies of derived model for solving (14) and (16)-(17) equations. The accuracy of the solver for relative and absolute errors are 0.0001 and 0.0001, respectively. The geometric parameters of the considered physical system are like Table I [6]. Note that this system fails the singular-free coupling condition (22) by having $r < R$, as shown in Example 1, which

TABLE I: Value of parameters for the simulation studies.

Variable	Value	Variable	Value
m_c	0.25 kg	r	0.131 m
M_b	1 kg	R	0.145 m
g	9.8 m/s ²	I_b	0.0140 kg·m ²

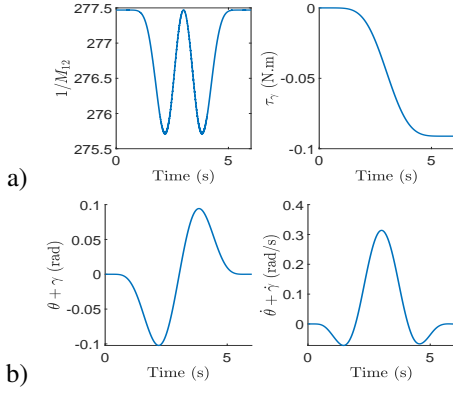


Fig. 6: a) Inertia term and output torque results for modified inverse dynamics, b) the true location and velocity of the rotating mass respect to reference frame.

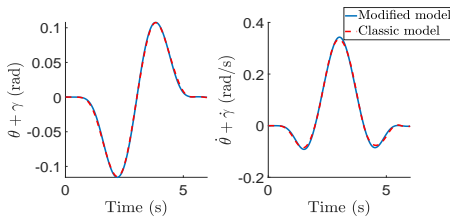


Fig. 7: Compared results for a classic and modified motion equations in a pendulum system with the inertia tensor I_c .

makes the system to be in a singular region. To prescribe the angular orientation of the spherical carrier the introduced Beta functions in (35) is applied where $k = \theta_{des}$ is 2 rad. The simulation is run for 6 s with $T = 6$. The robot begins from rest condition and by the prescribed Beta function it is expected to reach rest position at end of simulation time.

To solve the singularity, we utilize the proposed Theory 1 where a_i , n_i and ε_i are designed under the condition of (25). We chose a 3-phase ($l = 3$) waves with equal amplitude $a = a_1 = a_2 = a_3$ and frequency $n = n_1 = n_2 = n_3$ where $\Delta D_c = 0$. By substituting the values of the geometric parameters from Table into the conditions (25), we choose our combined waves parameters with first maximum value as $a = 0.01$ and $n = 3n' = 18$ which satisfy all three inequalities. Fig. 4 shows geometric shape of combined waves while our 3-phase curves have the phase angles $\varepsilon_i = (2\pi i)/3$ of $\{0, 2\pi/3, 4\pi/3\}$.

By running the simulation with obtained parameters, we see that the inverse dynamics are integrated without hitting any singularity [See Fig. 5-b and 6]. As expected, the rotating mass follows a smooth two-phase motion with the applied feed-forward control by the Beta function [see Fig. 6-b]. Also, the control torque τ_γ as the output is produced responsively with solving the modified nonlinear dynamics which displaces the spherical carrier to the desired location with the rest-to-rest motion.

Finally, we show a comparison between a classic rotating pendulum system with our modified singular-free model. All the simulation parameters are similar to the previous case-study except we include an inertia tensor of cylindrical pendulum $I_c = m_l r^2/3 = 0.0057 \text{ kg}\cdot\text{m}^2$ that is connected to the mass-point as Fig. 2. Also, we simulate the classic model of a pendulum system for the rolling sphere from

Refs. [4], [5] which same model can be derived by specifying $a = n = \varepsilon = 0$ at Eq. (14). Fig. 7 shows that our model doesn't have any dissimilarity with the classic model. In this case, note that inclusion of I_c variable satisfies the singular-free coupling condition in Eq. (24). We do this comparison for the sake of clarification that model with combined waves doesn't hurt/diverge the motion equations while it is removing the singularities due to coupling. Also, our designed theorem can easily work for all the geometries that singular-free coupling conditions was limited by (21) and (24) (worst-case as a mass-point) conditions in previous studies.

V. CONCLUSIONS

In this paper, we proposed a theory that designing the trajectory of the rotating mass via combined phase-shifted waves omits the singularities in the underactuated systems. We started with introducing the kinematics of the combined phase-shifted waves on the circular rotation of a mass-point. Next, the modified nonlinear dynamics of the underactuated rolling system were derived by Lagrangian equations. Before developing the condition for singularity-free inverse dynamics, the singularity regions relative to the geometric parametrization are shown for the spherical rolling systems. In the end, the solution of the theorem is demonstrated with example simulations where the states of the rolling carrier are specified by the Beta function.

As the advantage of our modified model, the solution is free from any complex algorithm or space transformation. This can resolve the limitations of the physical mechanism design due to the inertial coupling in the underactuated systems with 2 degrees of freedom. Also, it facilitates the applications of different advanced feedback controllers without any limited configurations. In the future, we plan to extend this theory for holonomic mechanisms with multiple degrees-of-freedom and we will check how can designing each passive constraint with various phase-shifted waves would prevent the integrated singular configurations.

REFERENCES

- [1] Y. Liu and H. Yu, "A survey of underactuated mechanical systems," *IET Control Theory A*, vol. 7, no. 7, pp. 921–935, 2013.
- [2] M. W. Spong and D. J. Block, "The pendubot: A mechatronic system for control research and education," in *Proc. IEEE Conf. Decis. Control.*, vol. 1, 1995, pp. 555–556.
- [3] M. W. Spong, "The swing up control problem for the acrobot," *IEEE Control Syst. Mag.*, vol. 15, no. 1, pp. 49–55, 1995.
- [4] E. Kayacan, Z. Y. Bayraktaroglu, and W. Saeys, "Modeling and control of a spherical rolling robot: a decoupled dynamics approach," *Robot.*, vol. 30, no. 4, pp. 671–680, 2012.
- [5] M. Svinin, Y. Bai, and M. Yamamoto, "Dynamic model and motion planning for a pendulum-actuated spherical rolling robot," in *Proc. IEEE Int. Conf. Robot. Autom.*, 2015, pp. 656–661.
- [6] S. A. Taffirishi, M. Svinin, E. Esmailzadeh, and M. Yamamoto, "Design, modeling, and motion analysis of a novel fluid actuated spherical rolling robot," *ASME J. Mech. Robot.*, vol. 11, no. 4, p. 041010, 2019.
- [7] S. A. Taffirishi, Y. Bai, M. Svinin, E. Esmailzadeh, and M. Yamamoto, "Inverse dynamics-based motion control of a fluid-actuated rolling robot," *Rus. J. Nonlin. Dyn.*, vol. 15, no. 4, pp. 611–622, 2019.
- [8] K. Ilin, H. Moffatt, and V. Vladimirov, "Dynamics of a rolling robot," *Proc. Natl. Acad. Sci. U.S.A.*, vol. 114, no. 49, pp. 12 858–12 863, 2017.
- [9] S. K. Agrawal, "Inertia matrix singularity of planar series-chain manipulators," in *Proc. IEEE Int. Conf. Robot. Autom.*, 1991, pp. 102–107.
- [10] H. Arai and S. Tachi, "Position control of manipulator with passive joints using dynamic coupling," *IEEE transactions on Robotics and Automation*, vol. 7, no. 4, pp. 528–534, 1991.

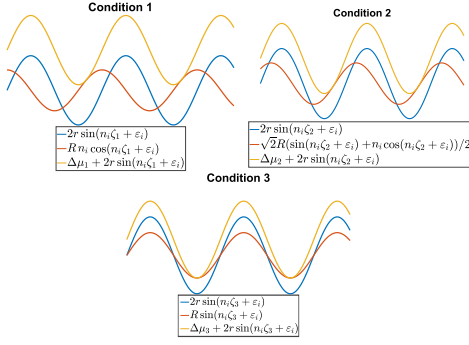


Fig. 8: An example for the minimum shift of each condition at (36) inequalities.

- [11] M. W. Spong, "Partial feedback linearization of underactuated mechanical systems," in *Proc. IEEE/RSJ Int. Conf. Intell. Robots Syst.*, vol. 1, 1994, pp. 314–321.
- [12] M. Bergerman, C. Lee, and Y. Xu, "A dynamic coupling index for underactuated manipulators," *Journal of Robotic Systems*, vol. 12, no. 10, pp. 693–707, 1995.
- [13] M. Zhang and T.-J. Tarn, "A hybrid switching control strategy for nonlinear and underactuated mechanical systems," *IEEE Trans. Autom. Control*, vol. 48, no. 10, pp. 1777–1782, 2003.
- [14] M. W. Spong, "Energy based control of a class of underactuated mechanical systems," *IFAC Proceedings Volumes*, vol. 29, no. 1, pp. 2828 – 2832, 1996, 13th World Congress of IFAC.
- [15] S. A. Taffirshi, M. Svinin, E. Esmailzadeh, and M. Yamamoto, "A fluid-actuated driving mechanism for rolling robots," in *The IEEE International Conference on Advanced Robotics and Mechatronics*, vol. 1, 2019, pp. 3527–3533.
- [16] A. Vretblad, *Fourier analysis and its applications*. Springer Science & Business Media, 2003, vol. 223.

COMPARISON OF THE SINUSOIDAL WAVES

In here, we find the required minimum shift for left-hand-side of inequality (32) to be always larger than the right-hand side of it. To find the required minimum shift for the i -th wave inequality sides, we first express the inverse Fourier Transform of (32) is calculated by (27) as follows

$$\begin{aligned}
 1) & 2ra_i \sin(n_i \zeta_1 + \varepsilon_i) > Ra_i n_i \cos(n_i \zeta_1 + \varepsilon_i) \\
 2) & 4ra_i \sin(n_i \zeta_2 + \varepsilon_i) > \sqrt{2}R \left[a_i \sin(n_i \zeta_2 + \varepsilon_i) \right. \\
 & \quad \left. + a_i n_i \cos(n_i \zeta_2 + \varepsilon_i) \right] \\
 3) & 2ra_i \sin(n_i \zeta_3 + \varepsilon_i) > Ra_i \sin(n_i \zeta_3 + \varepsilon_i)
 \end{aligned} \tag{36}$$

Next, we find the required shift for the first condition (there is $\pi/2$ phase difference between sides) with taking the derivative of time-domain forms in (36)

$$\frac{d}{d\zeta_1} \left[\frac{Rn_i \cos(n_i \zeta_1 + \varepsilon_i)}{2r \sin(n_i \zeta_1 + \varepsilon_i)} \right] = \frac{-Rn_i \sin(n_i \zeta_1 + \varepsilon_i)}{2r \cos(n_i \zeta_1 + \varepsilon_i)} = 1$$

Then, we solve it for $\gamma_1 = n_i \zeta_1 + \varepsilon_i$ and find the tangential point of two waves, when their slopes are the same,

$$\gamma_1 = \tan^{-1}(-2r/Rn_i), \tag{37}$$

Now, consider $\Delta\mu_1$ as the minimum required shift for the right-hand side of inequality to be always larger than left in condition 1 by equaling both sides as

$$\Delta\mu_1 + Ra_i n_i \cos(\gamma_1) = 2ra_i \sin(\gamma_1). \tag{38}$$

Next, we insert the γ_1 to (38) and re-order it which results the $\Delta\mu_1$ [see Fig. 8 as example] as

$$\begin{aligned}
 \Delta\mu_1 = & a_i \cdot \left| 2r \sin \left(\tan^{-1} \left(\frac{-2r}{Rn_i} \right) \right) \right. \\
 & \left. - Rn_i \cos \left(\tan^{-1} \left(\frac{-2r}{Rn_i} \right) \right) \right|.
 \end{aligned} \tag{39}$$

Condition 2 is also calculated similar to the first condition, but waves contain $\pi/4$ phase difference between each other due to the summed sine and cosine waves. Therefore, we take the derivative of computed Inverse Fourier

$$\begin{aligned}
 \frac{d}{d\zeta_2} \left[\frac{\sqrt{2}R[n_i \cos(n_i \zeta_2 + \varepsilon_i) + \sin(n_i \zeta_2 + \varepsilon_i)]}{4r \sin(n_i \zeta_2 + \varepsilon_i)} \right] \\
 = \frac{\sqrt{2}R[-n_i \sin(n_i \zeta_2 + \varepsilon_i) + \cos(n_i \zeta_2 + \varepsilon_i)]}{4r \cos(n_i \zeta_2 + \varepsilon_i)} = 1
 \end{aligned}$$

Next, the angle for tangent point on both curves $\gamma_2 = n_i \zeta_2 + \varepsilon_i$ is computed as

$$\gamma_2 = \tan^{-1} \left(\left(R - 2\sqrt{2}r \right) / Rn_i \right), \tag{40}$$

After knowing γ_2 , the minimum shift $\Delta\mu_2$ is calculated from waves in condition 2 as

$$\Delta\mu_2 + \frac{\sqrt{2}a_i}{2}R [\sin(\gamma_2) + a_i n_i \cos(\gamma_2)] = 2ra_i \sin(\gamma_2) \tag{41}$$

Substituting (40) into (41) results in $\Delta\mu_2$,

$$\begin{aligned}
 \Delta\mu_2 = & \frac{\sqrt{2}a_i}{2} \left| (2\sqrt{2}r - R) \sin \left(\tan^{-1} \left(\left(R - 2\sqrt{2}r \right) / Rn_i \right) \right) \right. \\
 & \left. - Rn_i \cos \left(\tan^{-1} \left(\left(R - 2\sqrt{2}r \right) / Rn_i \right) \right) \right|.
 \end{aligned} \tag{42}$$

The final condition in (36) is easy to compute because waves of both sides are in the same phase, hence, $\Delta\mu_2$ is obtained by maximum amplitude difference

$$\Delta\mu_3 = a_i \cdot |2r - R|. \tag{43}$$